Materials & Design 238 (2024) 112694

Contents lists available at ScienceDirect

Materials & Design

journal homepage: www.elsevier.com/locate/matdes

Biomimetic aligned nanofibrous dressings containing cell-selective polymer enhance diabetic wound regeneration

Erfan Rezvani Ghomi [a,b,c,d,m], Venkatesh Mayandi [b], Vijila Chellappan [c,*], Nileshkumar Dubey [e,f], Kottaiswamy Amuthavalli [d], Rasoul Esmaeely Neisiany [g,h], Veluchamy Amutha Barathi [b], Navin Kumar Verma [b,d,i,l,*], Rajamani Lakshminarayanan [b,j,k,*], Seeram Ramakrishna [a,*]

[a] Center for Nanotechnology and Sustainability, Department of Mechanical Engineering, National University of Singapore, Singapore 117581, Singapore
[b] Ocular Infections and Antimicrobials Research Group, Singapore Eye Research Institute, The Academia, 20 College Road, Discovery Tower, Singapore 169856, Singapore
[c] Institute of Materials Research and Engineering (IMRE), Agency for Science Technology and Research (A*STAR), 2 Fusionopolis Way, Innovis #08-03, Singapore 138634, Singapore
[d] Lee Kong Chian School of Medicine, Nanyang Technological University Singapore, Clinical Sciences Building, 11 Mandalay Road, Singapore 308232, Singapore
[e] Faculty of Dentistry, National University of Singapore, Singapore 119085, Singapore
[f] ORCHIDS: Oral Care Health Innovations and Designs Singapore, National University of Singapore, Singapore, Singapore 119085, Singapore
[g] Department of Polymer Engineering, Hakim Sabzevari University, Sabzevar 9617976487, Iran
[h] Biotechnology Centre, Silesian University of Technology, Krzywoustego 8 44-100, Gliwice, Poland
[i] National Skin Centre, 1 Mandalay Road, Singapore 308205, Singapore
[j] Ophthalmology and Visual Sciences Academic Clinical Program, Duke-NUS Medical School, Singapore 169857, Singapore
[k] Department of Pharmacy, National University of Singapore, Singapore 117559, Singapore
[l] Skin Research Institute of Singapore, Clinical Sciences Building, 11 Mandalay Road, Singapore 308232, Singapore
[m] A.J. Drexel Nanomaterials Institute, Drexel University, Philadelphia, PA 19104, United States

ARTICLE INFO

Keywords:
Electrospinning
Wound healing
Aligned nanofiber
Biomaterials
Bacterial infections

ABSTRACT

Diabetic ulcers remain a significant challenge in wound care due to loss of epithelial cell migration. Aligned nanofibrous scaffolds mimicking the skin's extracellular matrix (ECM) are promising candidates for diabetic wound healing. In this study, a composition of poly(ε-caprolactone), gelatin, and dopamine-containing varying amounts of ε-polylysine (ε-PL) was electrospun to prepare aligned nanofiber wound dressings (ANFDs). We then investigated the morphological, physicochemical, mechanical, and biological properties of fabricated ANDFs. The presence of ε-PL confers bactericidal properties while promoting epithelial and fibroblast adhesion, proliferation, and migration, confirming its cell selectivity. The clinical importance of the ANFDs was then demonstrated in a mice model of full-thickness diabetic wounds. The results confirm that ANFD treatment resulted in a higher rate of wound closure in the linear range of wound closure than wounds treated with silver dressings. Taken together, these results suggest the potential of antimicrobial ANFDs for the treatment of diabetic wounds.

1. Introduction

Diabetes mellitus is a common metabolic disease affecting over 400 million people worldwide. Patients with diabetes are highly susceptible to chronic wounds, such as diabetic ulcers and lesions, accounting for remarkable psychosomatic health and socioeconomic problems [1–3].

* Corresponding authors at: Institute of Materials Research and Engineering (IMRE), Agency for Science Technology and Research (A*STAR), #08-03, Singapore, 2 Fusionopolis Way, Innovis #08-03, Singapore 138634, Singapore (V. Chellappan), Lee Kong Chian School of Medicine, Nanyang Technological University Singapore, Clinical Sciences Building, 11 Mandalay Road, Singapore, 308232, Singapore (N.K. Verma), Ocular Infections and Antimicrobials Research Group, Singapore Eye Research Institute, The Academia, 20 College Road, Discovery Tower, Singapore 169856, Singapore (R. Lakshminarayanan), Center for Nanotechnology and Sustainability, Department of Mechanical Engineering, National University of Singapore, Singapore, 117581, Singapore (S. Ramakrishna).
E-mail addresses: c-vijila@imre.a-star.edu.sg (V. Chellappan), nkverma@ntu.edu.sg (N.K. Verma), lakshminarayanan.rajamani@seri.com.sg (R. Lakshminarayanan), seeram@nus.edu.sg (S. Ramakrishna).

https://doi.org/10.1016/j.matdes.2024.112694
Received 21 September 2023; Received in revised form 25 December 2023; Accepted 19 January 2024
Available online 24 January 2024

Table 1
The information of the ANFD samples.

Sample Code	ε-PL (wt. %)	Crosslinked
ANFD0	0	No
XL-ANFD0	0	Yes
ANFD5	5	No
XL-ANFD5	5	Yes
ANFD10	10	No
XL-ANFD10	10	Yes
ANFD15	15	No
XL-ANFD15	15	Yes

In diabetic patients, wound beds with rich glycemic grades provoke bacterial infections. Diabetic wounds with delayed or inappropriate medical care could cause significant ulceration, which in some cases leads to amputation, and eventually mortality [4,5]. The heightened prevalence of diabetic patients coupled with extended life expectancy has led to increased numbers of complications such as neuropathy and peripheral arterial disease which are the major risk factors for the development of diabetic foot ulcers. Microbial infections, co-morbidities, and the size and depth of the ulcer are the major reasons for delayed wound healing [6]. Owing to the potential complications and slower healing process, diabetic wounds require careful management.

Skin tissue engineering was among the initial organ systems to benefit from regenerative medicine techniques. Current research in skin tissue engineering is primarily focused on developing complex three-dimensional (3D) polymer scaffolds that contain functional biomolecules and can support cell growth [7]. Up to now, various types of wound dressings have been utilized to treat diabetic wounds [8,9]. The unique properties of human skin, such as impeding bacterial invasions, controlling the body temperature, and being selective to substance exchange, are some of the key attributes of wound dressings [10]. Electrospun nanofibrous mats have shown promise as wound dressings because of their ease of production, durable surface and topographical features of the nanofibers, and capabilities to incorporate various bioactive agents with immediate, sustained, or controlled release characteristics [11]. Moreover, electrospun nanofibrous mats mimic the dimensions of skin extracellular matrix (ECM), the natural environment in which cells reside, thus improving biocompatibility and their ease of application and conformability causing them to be ideal wound dressings for the management of diabetic wounds [12,13].

The antimicrobial agents used in contemporary wound dressings lack cell selectivity. Compounded by the increased evolution of antimicrobial resistance, there is an unmet clinical need for therapeutically safe and potent antimicrobials for the management of skin infections. We showed that ε-polylysine (ε-PL), a natural cationic antimicrobial polymer, has been proven to have effective antimicrobial performance against a wide range of pathogens, including Gram-negative and Gram-positive bacteria and fungi [14]. ε-PL is a linear homopolypeptide composed of almost 25–35 ε-L-lysine monomers. It should be noted that a polymeric chain of at least 10 L-lysine monomers is optimal for antimicrobial activity [15]. It has the US Food and Drug Administration (FDA) approval as an antimicrobial agent to be used as a food preservative [16]. ε-PL is biocompatible, biodegradable, hydrophilic, eco-friendly, and thermal-resistant and can be produced on an industrial scale [17]. According to the literature, ε-PL, with a molecular weight of 3600——4300 g/mol, showed higher antimicrobial performance, making it eligible as the bioactive agent in electrospun antimicrobial dressings [18,19].

In addition to the bioactive agents, the morphological properties of electrospun wound dressings are vital as effective wound dressings [13,20]. Directional cell migration plays an essential role in the wound-healing process. In fact, skin cells migrate into the wound environment toward collagen orientation. Lack of cell movement and unbridled cell migration could lead to clinical complications and wound healing failure [21]. Therefore, controlling cell migration is one of the main tasks of wound care. Conventional wound dressings, e.g., gauze and foam, mainly try to decrease the exudate and focus less on controlling cell behaviors, which may cause passive treatment or unforeseen inflammatory processes [22]. Thus, developing the manufacturing methods of

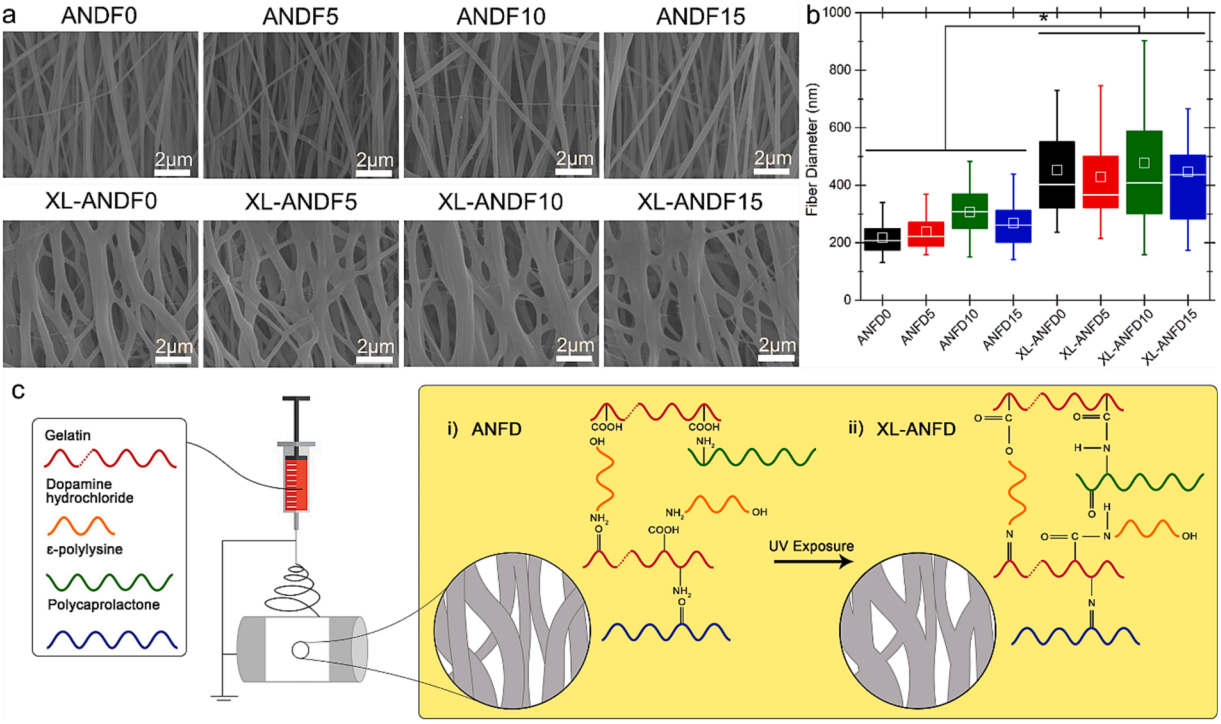

Fig. 1. Morphological assessment of ANFDs. (a) FE-SEM images of ANFD0, ANFD5, ANFD10, ANFD15, XL-ANFD0, XL-ANFD5, XL-ANFD10, and XL-ANFD15. Scale bar, 2 μm. (b) Distribution of nanofibers diameter for all samples (n = 50; *: $p < 0.05$). (c) Schematic illustration of the preparation of ANFDs and possible chemical reactions occurring during the UV crosslinking process.

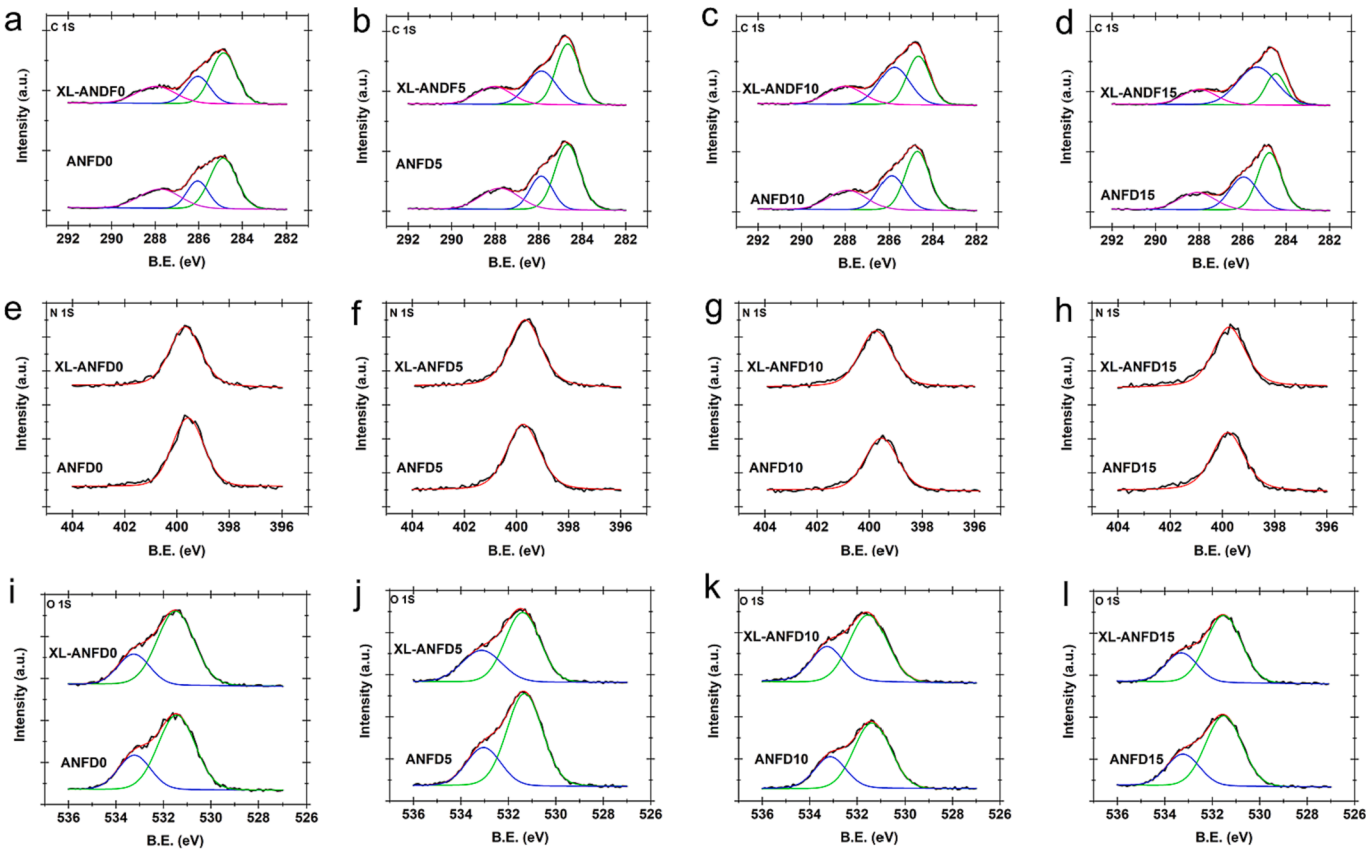

Fig. 2. XPS spectra of (a-d) C 1 s, (e-h) N 1 s, and (i-l) O 1 s, for both ANFDs and XL-ANFDs.

wound dressings that can help with cell migration is essential and desirable. Aligned nanofibrous mats have favorable properties for wound dressing application. Hence, various techniques have been developed to prepare electrospun aligned nanofibrous mats to provide desirable nanostructure, improved mechanical properties, and particularly cell alignment [11].

Biomaterials with specific topographic features would effectively manage cellular activities and have been utilized in tissue-engineered scaffolds [23]. Remarkably, patterns with aligned nanostructure can mimic human skin ECM, regulate cell orientation and migration, and improve wound healing. Among them, gelatin (Gel) is of great interest as it is highly biocompatible, FDA-approved, and biodegradable [24]. Gel enhances cell adhesion, proliferation, and wound healing properties [25]. Furthermore, synthetic and natural polymer blending is considered the most efficient method for achieving favorable composition for biomedical applications [26]. Following this method, the synthetic polymer primarily constitutes the backbone structure, while the natural polymer is in charge of the cell adhesion points and promotes cytocompatibility. Poly (ε-caprolactone) (PCL), a favored synthetic biopolymer, has good mechanical properties, but its hydrophobicity reduces its biocompatibility [27,28]. Therefore, blending Gel with PCL leads to a robust composite with improved cytocompatibility [29,30]. In our previous study, we varied the angular velocity of the rotating drum collector and determined the optimum degree of alignment for adhesion, migration, and proliferation of skin cells [12]. In this work, we determined the optimum antimicrobial and cell migration properties of the ANFDs with the highest degree of alignment and established their biocompatibility in a diabetic mice model of wound healing.

2. Experimental

2.1. Materials

PCL (Mn = 80,000 g/mol) as the synthetic polymer, Gel (porcine skin) as the natural polymer, 2,2,2-trifluoroethanol (TFE) as a solvent, dopamine hydrochloride (Dp) as the crosslinker, acetic acid (AA) as a solvent, formaldehyde, and Hoechst were provided from Sigma–Aldrich. ε-PL (Mw = 4,300 g/mol) as the antimicrobial agent was supplied by Hefei TNJ Chemical Industry Co. Ltd., China. In addition, both Muller-Hinton broth (MHB) and Mueller-Hinton agar (MHA) were obtained from BD (United States of America). The bacterial strains of *SA 15981 green fluorescent protein (gfp), EC 25922, AB 19606, PA O1 gfp, and MRSA 700699* were obtained by the American Type Culture Collection (ATCC) (United States of America). Phosphate-buffered saline (PBS) was obtained from Vivantis (Subang Jaya, Malaysia). Dulbecco's modified Eagle's medium (DMEM) and trypsin-EDTA were provided from Nacalai Tesque Inc., while fetal bovine serum (FBS) and Penicillin Streptomycin (Pen Strep) were available from the Gibco Life Technologies. Rhodamine-phalloidin was also purchased from Invitrogen™ for cell staining. CellTiter 96® AQ_{ueous} One Solution Reagent containing [3-(4,5-dimethylthiazol-2-yl)-5-(3-carboxymethoxyphenyl)-2-(4-sulfophenyl)–2H-tetrazolium, inner salt; MTS] was purchased from Promega for cell viability assay. The silicon culture inserts were purchased from Idibi for *in vitro* wound healing assay. Distilled water (DW) was used wherever required.

2.2. Fabrication of ANFDs

The electrospinning solutions were prepared based on the Gel:PCL: Dp (2:1:0.06 wt ratio) solution. Then, different amounts of ε-PL (5–15 wt %) were added to prepare the ANFDs, as shown in Table 1. First, Dp and

Table 2
Assigned spectral bands based on binding energy (BE) and atomic content (AC) for pristine and crosslinked electrospun mats.

Element	ANFD0		XL-ANFD0		ANFD5		XL-ANFD5		ANFD10		XL-ANFD10		ANFD15		XL-ANFD15		Assignments
	BE (eV)	AC (%)	BE (eV)	AC (%)	BE (eV)	AC (%)	BE (eV)	AC (%)	BE (eV)	AC (%)	BE (eV)	AC (%)	BE (eV)	AC (%)	BE (eV)	AC (%)	
C 1 s	284.87	32.92	284.85	31.44	284.67	34.77	284.64	30.99	284.71	32.51	284.67	26.76	284.76	32.14	284.48	17.36	**C–C or adventitious carbon**
C 1 s	286.04	14.30	286.04	22.19	285.88	16.03	285.82	24.71	285.88	19.78	285.76	26.86	285.95	21.82	285.34	38.48	**C–N, C = N, or C–O–C**
C 1 s	287.78	18.93	287.96	15.84	287.79	11.93	288.09	13.04	287.89	15.55	288	15.27	288.09	14.52	287.98	13.29	**C = O or O–C = O**
Total C		66.15		69.47		65.73		68.74		66.84		68.89		68.48		69.12	
O 1 s	531.4	16.92	531.49	15.73	531.32	16.18	531.4	13.66	531.37	16.12	531.54	13.81	531.51	13.96	531.52	13.03	**Organic –C = O**
O 1 s	533.07	6.35	533.26	4.75	533.07	6.19	533.12	6.98	533.12	6.57	533.26	7.08	533.23	5.68	533.3	6.37	**–C–O or OH**
Total O		23.26		20.48		22.37		20.64		22.69		21.07		19.63		19.40	
N 1 s	399.58	10.59	399.68	10.05	399.66	11.90	399.74	10.62	399.75	10.64	399.55	10.04	399.79	11.89	399.74	11.48	**N, C–NH_2**

ε-PL were dissolved in 6 mL DW. Second, Gel (1.8 g), TFE (5.4 mL), and AA (3.6 mL) were added to it (Solution 1). Third, PCL (0.9 g) was independently dissolved in TFE (5.4 mL) and AA (3.6 mL) (Solution 2). Fourth, both solutions 1 and 2 were combined using magnetic stirrers to merge homogenously and were left overnight. Then, the Nanon-01A machine (MECC Co. Ltd., Japan) was set on a voltage of 25 kV with a flow rate of 0.8 mL/h. The solutions were electrospun using a rotating cylindrical drum collector at 1,500 rpm. The electrospun mats were allowed to dry for two days in a fume hood. The dried mats were located in an ultraviolet (UV) crosslinker (Analytik Jena, United States of America) to initiate the cross-linking process through the polymerization of Dp. The mats were exposed to UV exposure of 7,500 μJ/s for three hours on each side [31].

2.3. Morphological analysis

A field emission scanning electron microscope (FESEM) (JEOL JSM 5600LV) was used to investigate the nanofibers' morphology both before and after the crosslinking process. Before imaging, the samples were coated with gold. Then, 50 single nanofibers were selected from the FESEM images of each sample (as shown in Table 1), and their average nanofiber diameter was measured by ImageJ software. In addition, an X-ray photoelectron spectroscope (XPS) (Kratos AXIS Ultra, Kratos Analytical Ltd.) was used to evaluate the chemical reactions that occurred during the crosslinking process from the surface of the samples.

2.4. Physico-mechanical properties assessment

The tensile properties of the electrospun mats were examined using a tensile tester (5542A, Instron) to assess the effect of different amounts of ε-PL on their tensile properties. The samples were prepared in rectangular strips of 20 × 10 mm^2. The samples were analyzed at a 2 mm/min tensile rate, room temperature, and ~ 50 % relative humidity. The test was conducted in both the vertical and alongside the fiber direction. Five strips of each sample in a specific direction were examined, and the average mechanical properties were reported.

The hydrophilicity of the samples was evaluated via the VCA Optima Surface Analysis System (AST Products Inc.). The samples' contact angle was measured via the sessile drop test at ~ 20 °C in the air with a drop (5 μL) of DW. The test was repeated in triplicates, and the average values were reported after one minute.

2.5. Antimicrobial performance

The antimicrobial performance of the electrospun mats was examined via the Kirby − Bauer radial disc diffusion method. First, MHA was prepared and poured into the Petri dishes to cover half of them, and then were left under the hood to solidify. Afterward, 10^6 CFU/mL of each bacterial strain was prepared, and 100 μL of it was spread on the surface of Petri dishes using a cotton swab. Next, the electrospun mats were cut in 1 × 1 cm^2, UV-sterilized for 1 h on each side, located in the middle of the MHA Petri dishes, and incubated at 37 ± 1 °C for 24 h. The results were reported by the mean value of inhibition zones from duplicate experiments.

Furthermore, the samples' antimicrobial activity was investigated by viability assay. Initially, the samples were prepared as mentioned above, soaked with 1 mL of bacterial strains (10^5 CFU/mL), and incubated for one day. Next, each bacterial strain suspension was serially diluted from 10^{-1} to 10^{-10} using NaCl buffer solution, and100 μL of each dilution was mixed with MHA to fill half of a sterile Petri dish and then incubated for 24 h. The experiment was duplicated for each dilution, and the results were presented by the changes in log reduction of viable colonies compared with the control sample. The control sample for each bacterial strain refers to the one which only includes bacteria (10^5 CFU/mL) and media without any of the prepared electrospun mats.

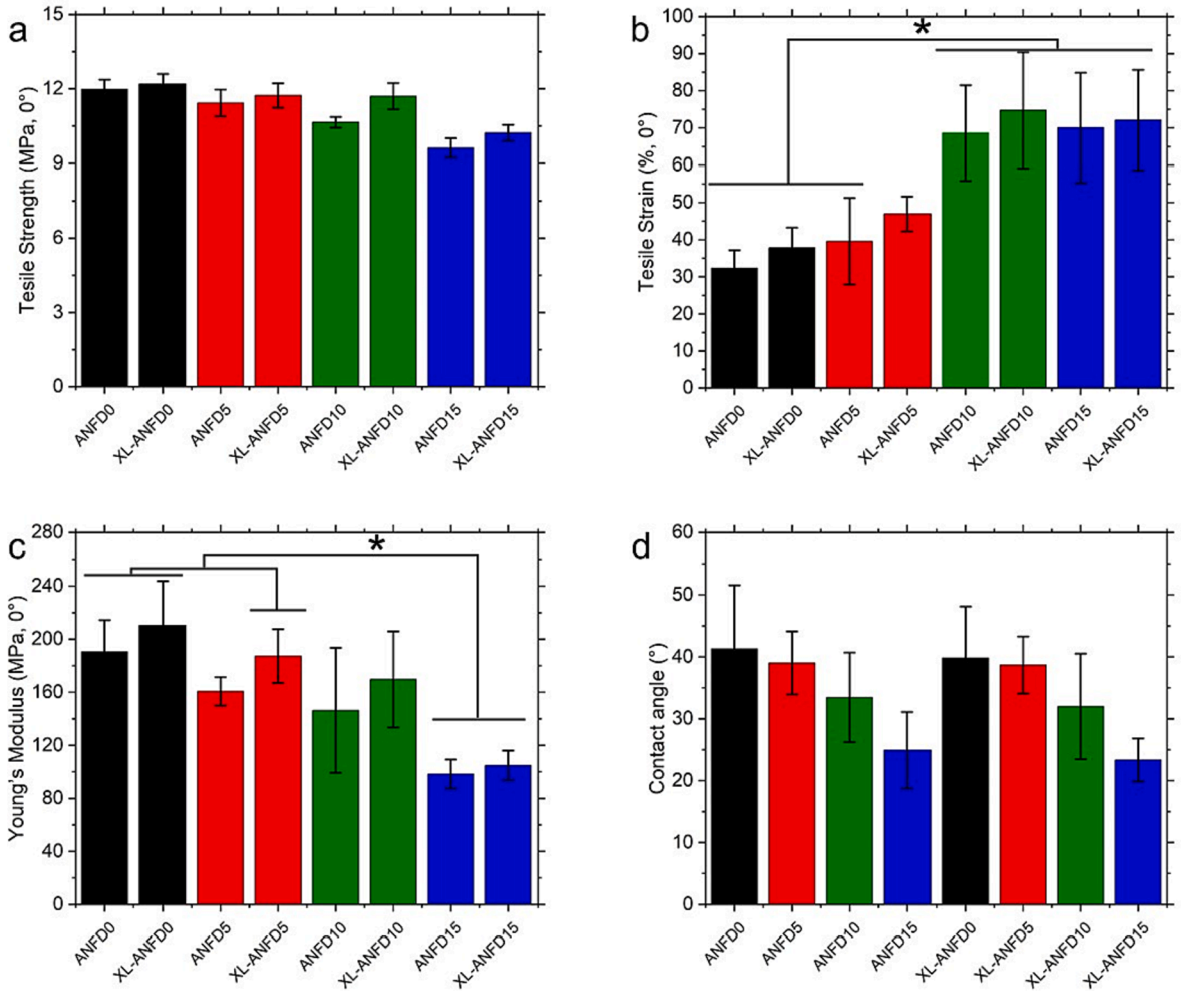

Fig. 3. Mechanical performance and wettability of ANFDs (0 degrees). (a) Tensile strength of the samples, (b) Tensile strain of the samples, (c) Young's modulus of the samples (n = 5, *: $p < 0.05$), and (d) The average contact angle values of the samples (n = 3).

2.6. In vitro assessment

Primary human dermal fibroblasts (hDFs) and keratinocytes (HaCaT cell line) were from the American Type Culture Collection (ATCC, Manassas, VA, USA). Cells were cultured in DMEM with 10 % FBS and 1 % Pen Strep (GIBCO). Cultures were tested free of mycoplasma on a routine basis using GeneCopoeia MycoGuard™. To determine the cytocompatibility of AFND preparations, they were collected on 14 mm coverslips (CS), sterilized by UV exposure, placed in the wells of 24-well plates, and stabilized by stainless steel O-rings. Wells containing AFND preparations were rinsed with the culture media before adding cells. Cells (1.5×10^4 cells/well in 500 μL medium) were seeded on the AFND preparations and allowed to grow for up to 7 days. Cells were seeded on sterilized CS as a control. To determine cell viability, 50 μL MTS reagents were added to the 1-day, 4-day, or 7-day cultured cells and incubated further for an additional 2 h. Viable cells convert MTS reagent into purple-colored products that were quantified by recording absorbance using a spectrophotometric reader (FLUOstar OPTIMA, BMG Lab Technologies) [32]. The total number of cells in each time point (1, 4, and 7 days) was calculated using the calibration curve from three independent experiments (Fig. S1).

Both hDFs and HaCaTs were first cultured for four days to assess their morphology on different samples [33]. Afterward, the cells were stabilized via 4 % formaldehyde for 15 mins, washed with PBS, and incubated in Rhodamine-Phalloidin and Hoechst for actin and nuclei, respectively, for 1 h [32]. Subsequently, cells were washed with PBS, attached to a glass slide, and imaged by Nikon Eclipse Ti (Nikon Instruments Inc, Melville). The image processing of triplicate experiments was done by Nikon NIS-Elements software.

A wound-healing assay was conducted to evaluate the effect of ε-PL concentration on cell migration and motility [34]. Fibroblasts and keratinocytes were seeded in the silicon insert gaps at 1.5×10^5 and 3×10^5 cells/well, respectively. The plates were then incubated for one day to let the cells attach, and after one day, the silicon inserts were removed to make an almost 500 μm cell-free gap. Subsequently, the culture media was changed to include 2 % FBS instead of 10 % to eliminate the cells and different concentrations of ε-PL (0, 0.5, 1, and 1.5 mg/mL). After one day, the cell migration was assessed via optical images at the cell-free area, and the healed area was calculated using ImageJ.

2.7. In-Vivo diabetic Full-Thickness wound healing assessment

In vivo studies were conducted using C57BL/6-*Ins2*^{Akita}/J mice that were approximately 8–9 weeks old and weighed between 20 and 30 g. The Akita colonies were purchased from Jackson Laboratory, and we expanded the colony by crossing Akita males with C57BL/6J females. The Akita strain is a model for studying phenotypes associated with type 1 diabetes. It is caused by a spontaneous mutation in the insulin 2 gene, which leads to incorrect folding of the insulin protein. This, in turn, produces toxicity in pancreatic beta cells, reduces beta cell mass, and results in reduced insulin secretion. Prior to surgery, the elevated blood glucose level of the mice was measured to monitor the onset of diabetes.

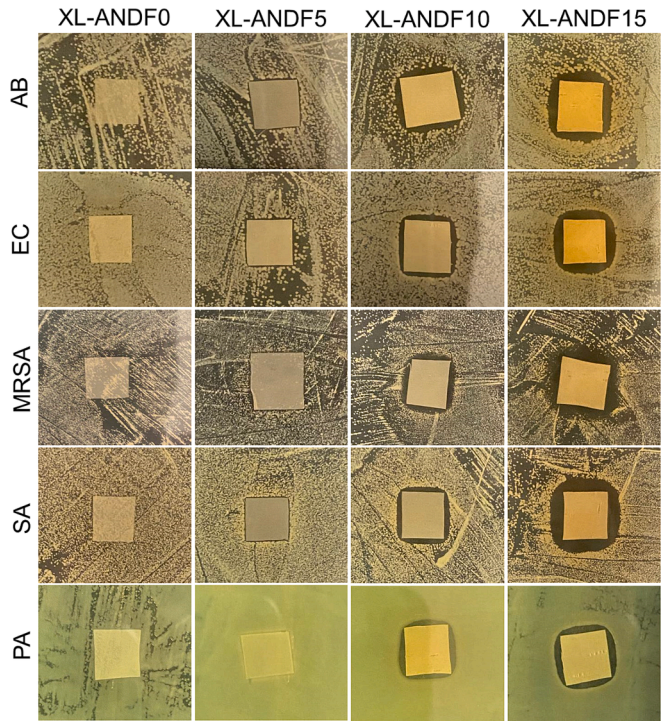

Fig. 4. Antimicrobial activity of XL-ANFDs via disc diffusion assay (n = 3). The abbreviations used are SA – *Staphylococcus aureus*; MRSA – *Methicillin-resistant Staphylococcus aureus*; PA – *Pseudomonas aeruginosa*; EC – *Escherichia coli*; and AB – *Acinetobacter baumannii*.

All experimental procedures were approved by the Institutional Animal Care and Use Committee (IACUC), Singapore Eye Research Institute. Mice were anesthetized using 5 % isoflurane in 100 % oxygen at a flow rate of 1 L/min and maintained it using 1–3 % isoflurane. The operative region of the mouse was shaved with an electric shaver and a hair removal cream (Veet) was applied on it. We then wiped the skin with an alcohol swab. To create middorsal full-thickness wounds, we used 8 mm biopsy punches (VWR) to excise the epidermis and dermis, including the panniculus carnosus, on either side of the midline. Wounds were covered with XL-ANFD10 or AQUACEL® Ag (comparative control) dressings and digital images of wounds were captured at days 0, 4, 8, 12, 16, and 21 after wounding. Images were analyzed using ImageJ software. The dressings were changed every 2 days until the endpoint 21 days post-wounding. A group of mice with no dressings was selected as the control group. Throughout the experiment, all animals were given ad libitum access to a chow diet and water.

2.8. Histological assessment

On day 21, mice were euthanized using CO_2 asphyxiation followed by cervical dislocation. The wounded back skin containing the large sheet was carefully excised from each mouse, bisected, and fixed using a 4 % paraformaldehyde solution for 24 h at 4 °C. Fixed tissues were then dehydrated in 70 % ethanol for 24 h at 4 °C, processed using a tissue processor (Leica Biosystems, HistoCore PEARL, Nussloch, Germany), and then embedded in paraffin. Tissue sections were cut into 5-μm thick sections using a rotary microtome (Leica Biosystems, RM2245, Germany).

Hematoxylin and eosin (H&E) staining was performed using an autostainer (Leica Biosystems, ST5010 Autostainer XL, Germany). To dewax, slides were submerged into the clearene solution twice for 5 min each. We then immersed the slides in 100 % ethanol twice for 2 min, followed by 95 % ethanol twice for 2 min and 70 % ethanol for 2 min. The tissues were dehydrated by rinsing them in a container of running tap water for 2 min.

Next, slides were submerged in the hematoxylin container for 1 min and excess dye was removed by rinsing with running tap water for 3 s. We then immersed the slides in the solution containing 0.3 % acid alcohol (0.3 % (v/v) concentrated hydrochloric acid, 70 % (v/v) ethanol, and 29.97 % (v/v) distilled water) to eliminate background staining. The hematoxylin-stained slides were dipped in Scott's tap water (0.5 % (w/v) sodium bicarbonate and 5 % (w/v) magnesium sulfate dissolved in distilled water) for 5 s to enhance the hematoxylin stain before rinsing with running tap water for 2 min.

After that, we immersed the sections in an alcoholic eosin solution for 2 min. We washed the eosin-stained sections with 70 % ethanol for 2 min, then twice for 2 min each with 95 % ethanol containers, twice for 2 min each with 100 % ethanol containers, and finally for 2 min with clearance to dehydrate the sections. We individually removed the stained slides, overlaid them with limonene, and sealed them using coverslips. H&E-stained images were acquired using a slide scanner (Carl Zeiss, Zeiss Axioscan Z1, Oberkochen, Germany) with a 20X

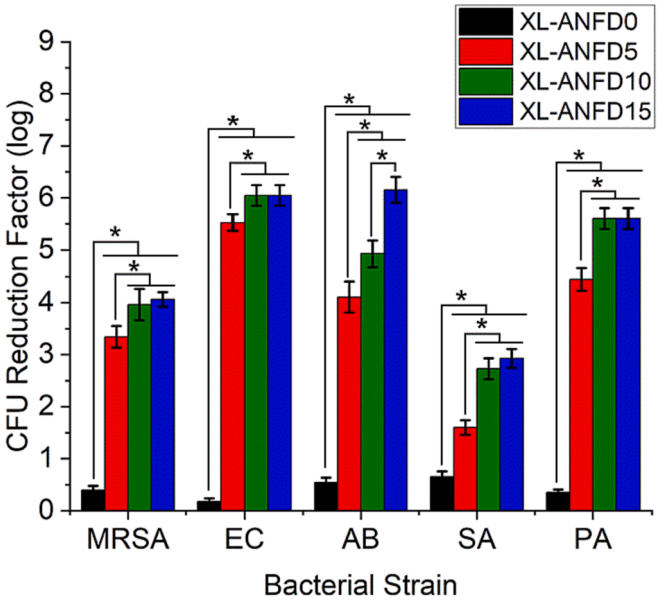

Fig. 5. Antimicrobial activity of ANFDs via viability assay; The abbreviations used are methicillin-resistant *Staphylococcus aureus* (MRSA), *Staphylococcus aureus* (SA), *Escherichia coli* (EC), *Acinetobacter baumannii* (AB), and *Pseudomonas aeruginosa* (PA) (n = 2; *: $p < 0.05$).

Table 3
Disc diffusion assay confirming the antimicrobial properties of ANFDs.

Sample	Inhibition zone diameter of bacterial strains (mm)				
	AB 19,606	*EC 25,922*	*MRSA 700,699*	*SA 15,981 gfp*	*PA O1 gfp*
XL-ANFD0	0	0	0	0	0
XL-ANFD5	10.69 ± 0.13	10.62 ± 0.18	10.12 ± 0.18	11.20 ± 0.49	10.53 ± 0.10
XL-ANFD10	13.01 ± 0.41	12.19 ± 0.41	12.78 ± 0.47	12.41 ± 0.81	12.99 ± 0.175
XL-ANFD15	14.22 ± 0.21	14.19 ± 0.38	14.69 ± 0.87	15.88 ± 0.22	12.77 ± 0.31

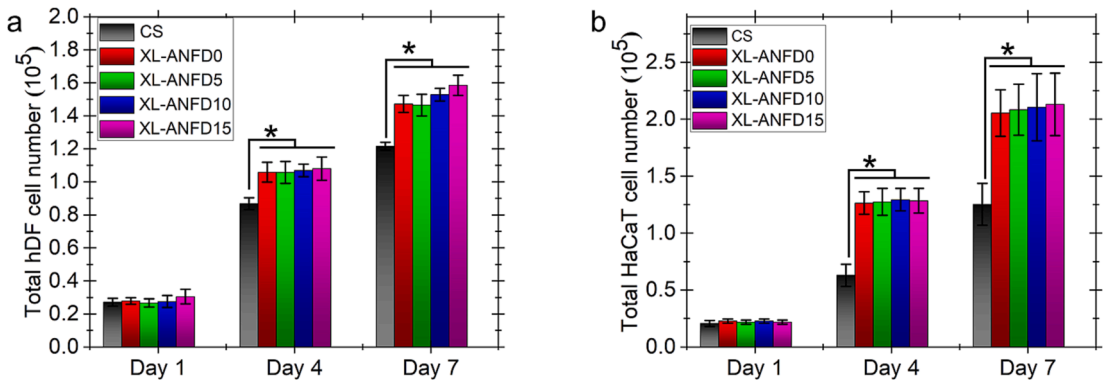

Fig. 6. Assessment of proliferation of human dermal fibroblasts and keratinocytes cultured on ANFDs. Cell proliferation of (a) hDF and (b) HaCaT cells at different time points (n = 3; *: $p < 0.05$).

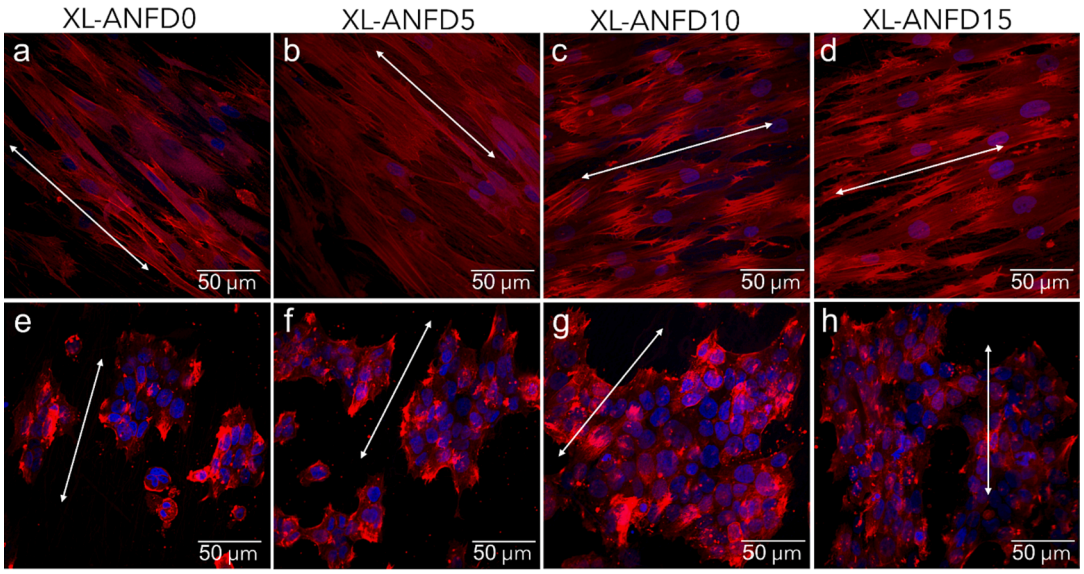

Fig. 7. Morphological evaluation of fibroblasts and keratinocytes. The images were taken after 4 days of incubation. Confocal images of hDF and HaCaT for (a, e) XL-ANFD0, (b, f) XL-ANFD5, (c, g) XL-ANFD10, (d, h) XL-ANFD15, respectively (Scale bar = 50 μm).

objective, and whole tissue sections were analyzed using Zeiss Zen Black software (Carl Zeiss, Germany).

2.9. Statistical Analysis

Analysis of variance (ANOVA) was exploited to analyze the data statistically where a "*p*" value less than 0.05 was regarded as significant.

3. Results and discussion

3.1. Morphological and physicochemical characterization of electrospun nanofibers

Preparation of scaffolds containing varying amounts of ε-PL presented aligned morphology of continuous fibers with no sign of beads (Fig. 1a). The mean fiber diameter for pristine nanofibers was 206–309 nm while for the crosslinked ones was 364–435 nm (Fig. 1b). These values are proximate to the collagenous skin ECM fibers [35], that support skin cell proliferation [11,35]. The diameter of nanofibers did not significantly change after adding various concentrations of ε-PL, as the changes in the composition of the solutions did not substantially affect their viscoelastic properties [35], and crosslinking could improve the durability and mechanical properties of ANFDs, as reported earlier [36]. FE-SEM images demonstrated the efficacy of the UV crosslinking method due to changes in the morphological properties of the samples. The larger nanofiber diameter for XL-ANFDs, which can be attributed to the formation of new covalent bonding, leads to the fusion among fibers. The covalent bonds formed among the functional groups correspond to the formation of polydopamine coating and crosslinking (Fig. 1c) [12]. In addition, as all the samples have an aligned morphology, they will provide a desirable nanostructure for dermal fibroblasts to be more active, which leads to a more favorable condition for the actin cytoskeleton to promote wound healing [37,38]. Hence, the ANFDs mimic the skin ECM and are beneficial in boosting the speed of wound healing and shortening the treatment period [39].

XPS was carried out for all ANFD samples by marking the high-resolution spectra of O 1 s, C 1 s, and N 1 s peaks (Fig. 2). The oxygen and carbon spectra were subdivided into two and three different peaks, respectively, while the nitrogen spectrum was fitted with one curve. The results of each spectrum at their specific binding energies (BEs) are presented in Table 2. The total atomic concentration (AC) of carbon increased during UV exposure, confirming the crosslinking process [40]. Considering the carbon peak at ~ 286 eV for all ANFDs, the AC significantly surged after crosslinking, which can be justified by the formation of new functional groups to contain C–N or C–O–C. Moreover, the other reason for the increase in AC of carbon at ~ 286 eV and total C is due to

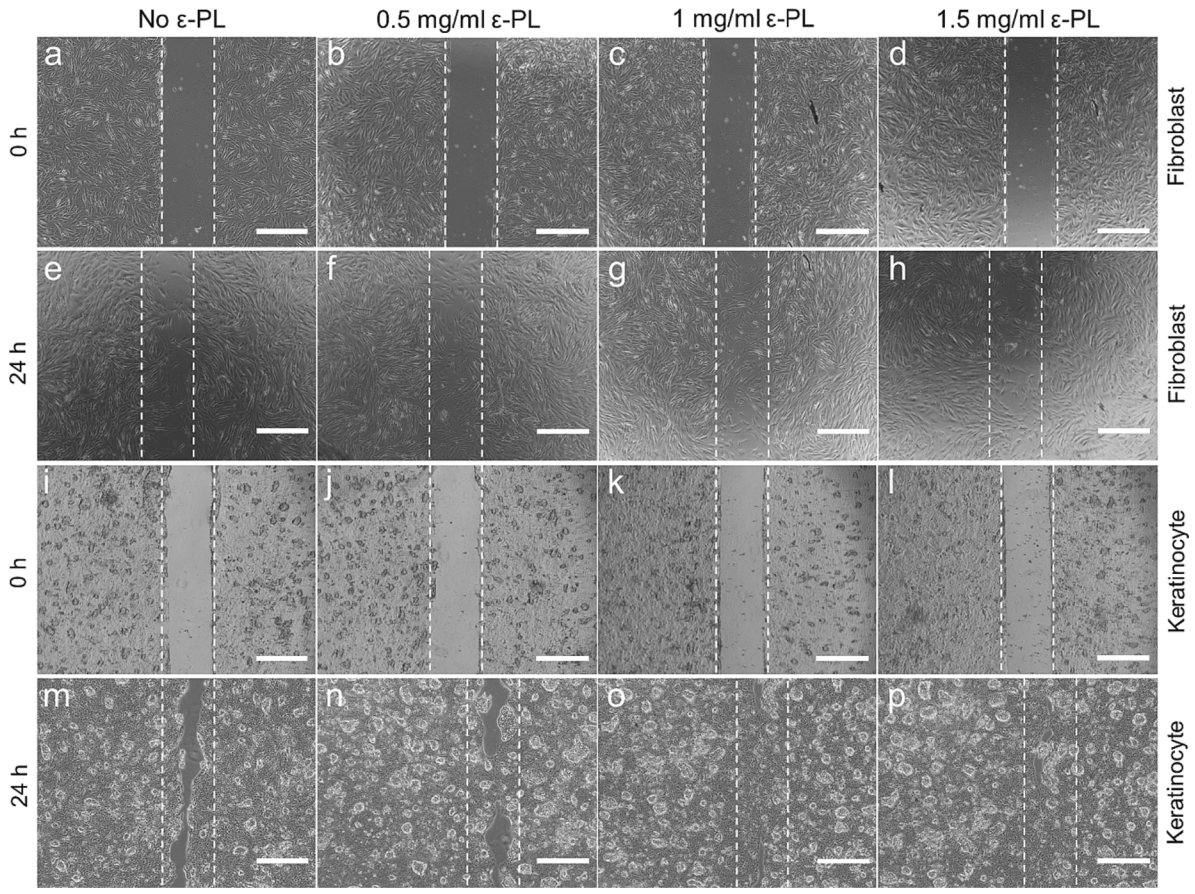

Fig. 8. Effect of the addition of ε-PL on dermal cell migration. (a-h) Fibroblast and (i-p) keratinocyte migration assays. The spotted white lines demarcate the wound borders at 0 h (Scale bar = 800 μm. n = 3; *: $p < 0.05$).

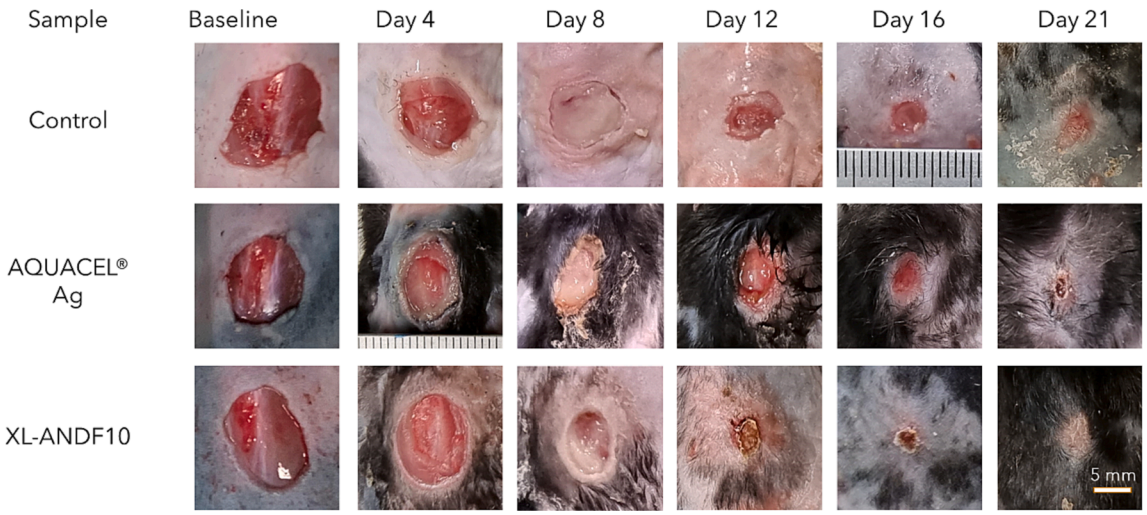

Fig. 9. Gross imaging of wound healing process for the untreated wound (control) and the wounds treated with AQUACEL® Ag and XL-ANFD10 over 21 days (n = 5).

the increased amount of C = N because of the addition of ε-PL [32]. On the other hand, the nitrogen spectrum witnessed a slight decrease in its AC after crosslinking for all ANFDs, which can be because of the possible reactions that occurred between NH_2 and COOH [12]. In the same way, the AC of oxygen peak at ~ 531 eV, corresponding to C = O, decreased with the addition of ε-PL, where the ANFD0 and XL-ANFD15 showed the highest (23.26 %) and lowest (19.4 %) amounts of total O, respectively. The decrease in C = O and the increase in C = N affirmed crosslinking between polydopamine and Gel/ε-PL. Practically, the causes of additional C = N bonding are either the reaction of the -C = O groups of Dp and $–NH_2$ groups of Gel during crosslinking or the possible bonding between $–NH_2$ and -C = O groups of ε-PL with both Gel and Dp [41,42].

3.2. Mechanical performance and wettability of the ANFDs

Wound dressings require mechanical strength to ascertain

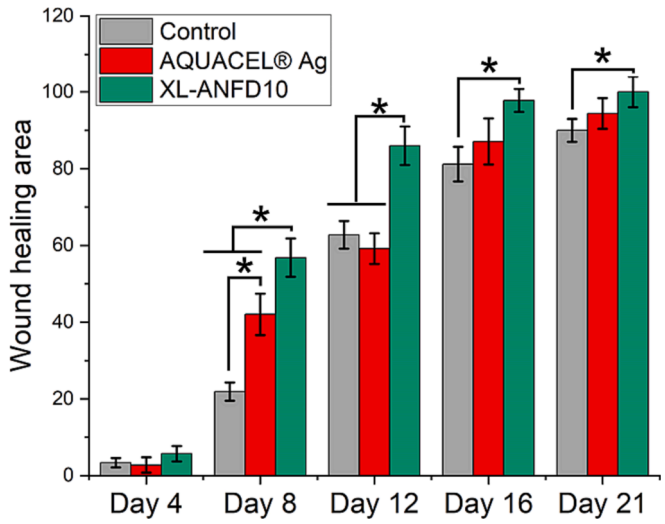

Fig. 10. Wound healing area for the untreated wound (control) and the wounds treated with AQUACEL® Ag and XL-ANFD10 during 21 days (n = 5, *: $p < 0.05$).

appropriate flexibility, robustness, and stress resistance to tolerate movement tensions and stresses during application and usage [43]. The mechanical performance of the ANFDs was assessed in both the parallel and vertical directions with respect to the alignment angle to check the effect of the increase in the drug concentration and crosslinking process (Fig. 3a–c and Fig. S2). By increasing the concentration of ε-PL, a slight decrease in tensile strength and a considerable reduction in Young's modulus were observed, while the tensile strain of the samples significantly increased. Due to the low molecular weight of ε-PL compared to Gel, by increasing the concentration of ε-PL, the molecular mass of the electrospun mats decreases, which weakens the intermolecular bonds of the samples and hence, reduces the tensile strength. In addition, ε-PL is considered a plasticizer in which by increasing its concentration, the tensile strain increases and Young's modulus decreases [44]. Moreover, crosslinking of the ANFDs helped with higher mechanical strength due to the formation of new covalent bonding during the UV crosslinking process [45]. These results are also consistent with our previously reported findings [12,32].

The wettability of a wound dressing is considered a key factor for its cytocompatibility and other cell functionalities and is reported by the contact angle of the wound dressing [46]. Hydrophobic surfaces lead to less cell adhesion, particularly in the first step of cell culture [46]. Fig. 3d shows the contact angle of ANFDs which all were below 90 degrees, demonstrating their hydrophilic surface. By increasing the concentration of ε-PL, the contact angle of the sample decreased, which could be due to the increase in the number of functional groups of the sample rendering them hydrophilic. Furthermore, the UV crosslinking process of ANFDs did not considerably change their wettability [47].

3.3. Antimicrobial activity of the ANDFs

One of the most critical characteristics of an ideal antibacterial wound dressing is its capability to inhibit the commencement of infections in wound environments [48]. Therefore, it is essential to make sure that the incorporation of ε-PL in the polymeric matrix does not affect its antimicrobial properties and the amount needed. Indeed, the incorporation of ε-PL considerably promoted the antimicrobial performance of the ANFDs and showed a clear zone of inhibition (ZOI) against all the tested bacterial strains (Fig. 4). Increasing concentrations of ε-PL in the ANFDs increased the ZOI. Since the polymeric matrix of PCL, Gel, and Dp did not show any antimicrobial effect [49], it can be concluded that all the antimicrobial performance of the samples stems from the presence of ε-PL and no loss of activity after crosslinking treatment. Table 3 presents the disk diffusion assay results against *AB 19606*, *EC 25922*, *MRSA 700699*, *SA 15981 gfp,* and *PA O1 gfp*. In a previous study, we showed that the crosslinking process does not affect the antimicrobial properties of ANFDs [12].

In addition, all ANFD preparations showed a considerable reduction in the CFU count for the tested pathogens (Fig. 5). The CFU reduction for all bacterial strains increased with the increase in the ε-PL concentration. Samples containing 10 and 15 wt% of ε-PL showed similar results and reduced the CFU factor by 2 to 6 $\log_{10}$ reduction, depending on the nature of bacterial isolates. ANFDs with an ε-PL concentration of more than 10 wt% could completely eradicate both gram-positive and gram-

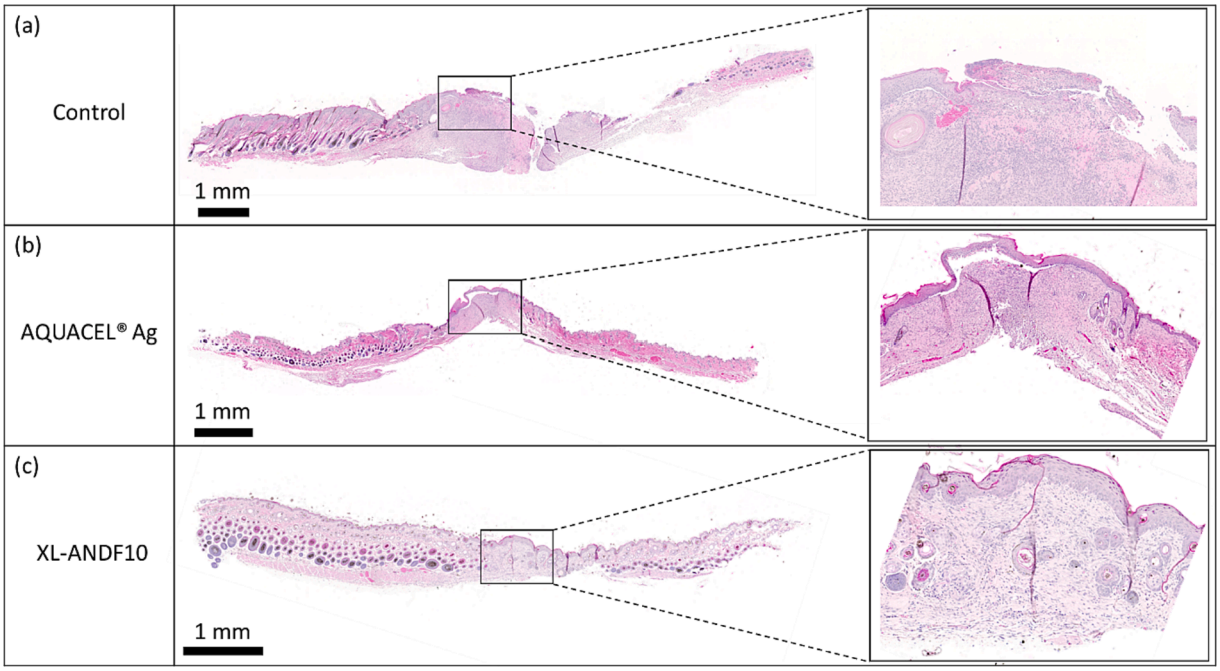

Fig. 11. Representative images of H&E-stained tissue sections of wounds treated with no dressing, with AQUACEL® Ag, and with XL-ANFD10 on day 21 (n = 5).

negative ATCC strains. The viability assay results indicate the high potential of the ANFDs tested. Gram-negative bacteria were more susceptible than Gram-positive pathogens.

3.4. Cytocompatibility evaluation of ANFDs

Proper contact with non-cytotoxic wound dressings facilitates epithelial and fibroblast cell proliferation and enhances re-epithelialization on wounds [50]. Commercial antimicrobial wound dressings containing silver exhibit substantial toxicity for skin cells in the initial stages of usage because of exploiting the boosted dose of antibacterial agents [51]. To verify the cytocompatibility of ANFDs and find the appropriate dosage of the ε-PL, HaCaT, and hDF cells were seeded on crosslinked ANFDs containing varying amounts of ε-PL. An MTS-based assay was used to quantify cell proliferation at various time points - one day, four days, and seven days. The cell numbers of both HaCaT and hDF cell lines were calculated and are presented (Fig. 6). We found that all the ANFDs containing varying amounts of ε-PL (5 %, 10 %, or 15 %) were cytocompatible to dermal fibroblasts and keratinocytes as there were no major signs of cytotoxicity among cells growing on ANFD preparations. Cell numbers of both cell types cultured on ANFDs were almost equal to or higher than the control.

Fig. 7 shows the confocal images of fibroblasts and keratinocytes on adherent ANFDs containing varying amounts of ε-PL. hDFs were aligned with respect to the direction of the nanofiber alignment (Fig. 7a, d). Similarly, HaCaT microcolonies were observed in aligned morphologies (Fig. 7e–h). As reported in our previous publication, 1,500 rpm is sufficient to achieve cell alignment in the nanofibers' direction [12]. The aligned morphology of the nanofibers leads to the cell alignment that induces bipolar properties in the cells and facilitates spacing to accommodate a higher number of cells compared to randomly oriented fibers [52]. Morphological observations were consistent with cell proliferation results and demonstrated the remarkable cytocompatibility of the ε-PL-incorporated nanofibers for skin cells.

3.5. Cell migration of ANFDs

After seeding the fibroblasts and keratinocytes into the gaps of the silicon inserts, a confluent layer of cells and a cell-denuded gap on the surface of ANFDs were observed (Fig. 8a–d and i–l). Then, to demonstrate the effect of the addition of ε-PL on the migration of dermal cells, the well-plates media was changed to contain various amounts of ε-PL (0.5, 1, and 1.5 mg/ml). After 24 h, the motility of hDF and HaCaT cells was visualized under an optical microscope. For HDFs, the gaps in the wells containing 0.5 – 1.5 mg/ml of ε-PL were fully closed. On the other hand, complete closure of the gap for HaCaT was observed for media supplemented with 1 and 1.5 mg/ml of ε-PL. Compared to the well without ε-PL, it can be concluded that the addition of ε-PL could accelerate the migration of both skin cells [33,53,54].

3.6. In-Vivo diabetic full-thickness wound healing assessment

To test our hypothesis that XL-ANFD10 dressing might expedite wound healing in diabetic mice, a full-thickness wound was created on the back of each mouse. During the 21-day treatment period, no adverse reactions, such as infection, were seen in any of the animals. Fig. 9 displays the macroscopic changes in the wound areas treated with the blank, AQUACEL® Ag and XL-ANFD10, on the 4th, 8th and 12th, 16th, and 21st postoperative days. The wound size decreased for all the groups but with significant differences in the rate of wound healing. On day 8, all samples exhibited a considerable decrease in wound size, and XL-ANFD10 showed a significant decrease in comparison to untreated or AQUACEL® Ag treated wounds. At day 12 post-injury, ~90 % wound closure was observed for the wounds treated with XL-ANFD10 when compared to the untreated or AQUACEL® Ag treated wounds. It should be noted that on day 12, the wounds from the control group and AQUACEL® Ag's group appeared wet and open (Fig. 9). It is likely that the alignment of the nanofibers promoted cell migration and eventually led to faster wound closure, which agrees with previous works [12,55]. On day 16, there is a significant difference in the wound area between control and XL-ANFD10 wounds (Fig. 10). Although the wounds on day 21 for all groups are closed and seemed to be healed, there is no sign of scar or wound in XL-ANFD10′s group which is promising for its clinical use.

H&E staining of the excised skin is shown in Fig. 11. As can be seen, the epidermis, dermis, hypodermis, and collagen fibers of the untreated group (control) displayed poorly defined structure at day 21 post-injury. However, wounds treated with AQUACEL® Ag show a full closure of the wound with less intact epidermis formed (Fig. 11b). The group receiving XL-ANFD10 treatment showed the development of new skin appendages accompanied by a smooth re-epithelialization of the wounded tissue (Fig. 11c). Moreover, on day 21 the wound treated with XL-ANFD10 showed a significantly larger number of hair follicles compared with those treated with blank and AQUACEL® Ag (Fig. 11c), suggesting enhanced regeneration of the tissue. This might be attributed to the XL-ANFD10 improved hydrophilicity, increased number of cell recognition sites, and antibacterial activity given by ε-PL that promote fibroblast and keratinocyte survival and proliferation during wound healing. As a result, this innovative XL-ANFD10 wound dressing has a high potential for the management of diabetic wounds.

4. Conclusions

The present study demonstrated the changes in mechanical and antimicrobial properties of aligned and crosslinked PCL/Gel nanofibers containing various concentrations of ε-PL. The results suggest that XL-ANFD10 which contained 10 % ε-PL displayed optimum mechanical strength and wettability. Antimicrobial assays indicated $> 2\log_{10}$ reduction in the viability of bacteria upon exposure to XL-AFND10 that colonizes the skin tissues of diabetic patients. The dressings promoted the adhesion, proliferation, migration, and polarization of keratinocytes and fibroblasts. These observations indicate that the polymer is highly selective in targeting microbial cells and does not interfere with the cellular activities of the skin cells. In a diabetic mice model of full-thickness wounds, XL-ANFD10 accelerated wound healing by enhanced re-epithelialization and granulation. In summary, our results highlight the translational relevance of the dressings for the treatment of diabetic wounds.

CRediT authorship contribution statement

Erfan Rezvani Ghomi: Conceptualization, Data curation, Formal analysis, Investigation, Methodology, Validation, Visualization, Writing – original draft, Writing – review & editing. **Venkatesh Mayandi:** Conceptualization, Methodology, Validation, Visualization. **Vijila Chellappan:** Conceptualization, Investigation, Resources, Supervision, Validation, Writing – review & editing. **Nileshkumar Dubey:** Conceptualization, Methodology, Validation, Writing – review & editing. **Kottaiswamy Amuthavalli:** Data curation, Investigation, Methodology. **Rasoul Esmaeely Neisiany:** Conceptualization, Investigation, Methodology, Validation, Writing – review & editing. **Veluchamy Amutha Barathi:** . **Navin Kumar Verma:** Conceptualization, Investigation, Methodology, Supervision, Validation, Writing – review & editing. **Rajamani Lakshminarayanan:** Conceptualization, Formal analysis, Investigation, Methodology, Resources, Supervision, Validation, Writing – review & editing. **Seeram Ramakrishna:** Investigation, Resources, Supervision, Validation, Writing – review & editing.

Declaration of competing interest

The authors declare that they have no known competing financial interests or personal relationships that could have appeared to influence

the work reported in this paper.

Data availability

Data will be made available on request.

Acknowledgments

RL thanks funding support from the Singapore Ministry of Health's National Medical Research Council under its Centre Grant Program (MOH-001001-00) and Open Funding—Independent Research Grant (MOH-000963-00). N.K.V. acknowledges funding support from the Singapore Ministry of Education (MOE) under its MOE Academic Research Fund (AcRF) Tier 1 Grant (RG94/22).

Appendix A. Supplementary data

Supplementary data to this article can be found online at https://doi.org/10.1016/j.matdes.2024.112694.

References

[1] F.L. Bowling, S.T. Rashid, A.J.M. Boulton, Preventing and treating foot complications associated with diabetes mellitus, Nat. Rev. Endocrinol. 11 (10) (2015) 606–616.
[2] Y.-J. Fu, Y.-F. Shi, L.-Y. Wang, Y.-F. Zhao, R.-K. Wang, K. Li, S.-T. Zhang, X.-J. Zha, W. Wang, X. Zhao, W. Yang, All-Natural immunomodulatory bioadhesive hydrogel promotes angiogenesis and diabetic wound healing by regulating macrophage heterogeneity, Adv. Sci. 10 (13) (2023) 2206771.
[3] D. Ailincai, S. Cibotaru, A. Anisiei, C.G. Coman, A.S. Pasca, I. Rosca, A.-I. Sandu, L. Mititelu-Tartau, L. Marin, Mesoporous chitosan nanofibers loaded with norfloxacin and coated with phenylboronic acid perform as bioabsorbable active dressings to accelerate the healing of burn wounds, Carbohydr. Polym. 318 (2023) 121135.
[4] W.J. Jeffcoate, K.G. Harding, Diabetic foot ulcers, Lancet 361 (9368) (2003) 1545–1551.
[5] L. Wang, G. Chen, L. Fan, H. Chen, Y. Zhao, L. Lu, L. Shang, Biomimetic enzyme cascade structural color hydrogel microparticles for diabetic wound healing management, Adv. Sci. 10 (14) (2023) 2206900.
[6] L. Wu, G. Norman, J.C. Dumville, S. O'Meara, S.E.M. Bell-Syer, Dressings for treating foot ulcers in people with diabetes: an overview of systematic reviews, Cochrane Database of Systematic Reviews (7) (2015).
[7] S. Chung, C.J. Koh, 56 - Fetal Tissues, in: A. Atala, R. Lanza, J.A. Thomson, R. M. Nerem (Eds.), Principles of Regenerative Medicine, Academic Press, San Diego, 2008, pp. 968–977.
[8] Y. Zhang, J. Zhou, Y. Zhang, D. Zhang, K.T. Yong, J. Xiong, Elastic fibers/fabrics for wearables and bioelectronics, Adv. Sci. 9 (35) (2022) 2203808.
[9] H. Liu, R. Chen, P. Wang, J. Fu, Z. Tang, J. Xie, Y. Ning, J. Gao, Q. Zhong, X. Pan, D. Wang, M. Lei, X. Li, Y. Zhang, J. Wang, H. Cheng, Electrospun polyvinyl alcohol-chitosan dressing stimulates infected diabetic wound healing with combined reactive oxygen species scavenging and antibacterial abilities, Carbohydr. Polym. 316 (2023) 121050.
[10] C. Korupalli, H. Li, N. Nguyen, F.-L. Mi, Y. Chang, Y.-J. Lin, H.-W. Sung, Conductive materials for healing wounds: their incorporation in electroactive wound dressings, characterization, and perspectives, Adv. Healthc. Mater. 10 (6) (2021) 2001384.
[11] E. Rezvani Ghomi, F. Khosravi, R.E. Neisiany, M. Shakiba, M. Zare, R. Lakshminarayanan, V. Chellappan, M. Abdouss, S. Ramakrishna, Advances in electrospinning of aligned nanofiber scaffolds used for wound dressings, current opinion, Biomed. Eng. 22 (2022) 100393.
[12] E.R. Ghomi, R. Lakshminarayanan, V. Chellappan, N.K. Verma, A. Chinnappan, R. E. Neisiany, K. Amuthavalli, Z.S. Poh, B.H.S. Wong, N. Dubey, R. Narayan, S. Ramakrishna, Electrospun Aligned PCL/Gelatin scaffolds mimicking the skin ecm for effective antimicrobial wound dressings, Advanced Fiber Materials 5 (1) (2023) 235–251.
[13] A. Memic, T. Abdullah, H.S. Mohammed, K. Joshi Navare, T. Colombani, S. A. Bencherif, latest progress in electrospun nanofibers for wound healing applications, ACS Applied Bio Materials 2 (3) (2019) 952–969.
[14] B.A. Pati, W.E. Kurata, T.S. Horseman, L.M. Pierce, Antibiofilm activity of chitosan/epsilon-poly-L-lysine hydrogels in a porcine ex vivo skin wound polymicrobial biofilm model, Wound Repair Regen. 29 (2) (2021) 316–326.
[15] Q. Yang, Z. Xie, J. Hu, Y. Liu, Hyaluronic acid nanofiber mats loaded with antimicrobial peptide towards wound dressing applications, Mater. Sci. Eng. C 128 (2021) 112319.
[16] X. Lan, Y. Liu, Y. Wang, F. Tian, X. Miao, H. Wang, Y. Tang, Coaxial electrospun PVA/PCL nanofibers with dual release of tea polyphenols and ε-poly (L-lysine) as antioxidant and antibacterial wound dressing materials, Int. J. Pharm. 601 (2021) 120525.
[17] N.A. Patil, B. Kandasubramanian, Functionalized polylysine biomaterials for advanced medical applications: a review, Eur. Polym. J. 146 (2021) 110248.
[18] R. Wang, B. Zhou, D.-L. Xu, H. Xu, L. Liang, X.-H. Feng, P.-K. Ouyang, B. Chi, Antimicrobial and biocompatible ε-polylysine–γ-poly(glutamic acid)–based hydrogel system for wound healing, J. Bioact. Compat. Polym. 31 (3) (2016) 242–259.
[19] Y. Xi, J. Ge, Y. Guo, B. Lei, P.X. Ma, Biomimetic elastomeric polypeptide-based nanofibrous matrix for overcoming multidrug-resistant bacteria and enhancing full-thickness wound healing/skin regeneration, ACS Nano 12 (11) (2018) 10772–10784.
[20] X. Zhang, L. Li, J. Ouyang, L. Zhang, J. Xue, H. Zhang, W. Tao, Electroactive electrospun nanofibers for tissue engineering, Nano Today 39 (2021) 101196.
[21] A. Ahmadi, P. Ahmadi, M.A. Sani, A. Ehsani, B. Ghanbarzadeh, Functional biocompatible nanocomposite films consisting of selenium and zinc oxide nanoparticles embedded in gelatin/cellulose nanofiber matrices, Int. J. Biol. Macromol. 175 (2021) 87–97.
[22] L. Mao, S. Hu, Y. Gao, L. Wang, W. Zhao, L. Fu, H. Cheng, L. Xia, S. Xie, W. Ye, Z. Shi, G. Yang, Biodegradable and Electroactive regenerated bacterial cellulose/MXene (Ti3C2Tx) composite hydrogel as wound dressing for accelerating skin wound healing under electrical stimulation, Adv. Healthc. Mater. 9 (19) (2020) 2000872.
[23] L. Zhu, D. Luo, Y. Liu, Effect of the nano/microscale structure of biomaterial scaffolds on bone regeneration, Int. J. Oral Sci. 12 (1) (2020) 6.
[24] J. Comelles, V. Fernández-Majada, N. Berlanga-Navarro, V. Acevedo, K. Paszkowska, E. Martínez, Microfabrication of poly(acrylamide) hydrogels with independently controlled topography and stiffness, Biofabrication 12 (2) (2020) 025023.
[25] I. Garcia-Orue, E. Santos-Vizcaino, A. Etxabide, J. Uranga, A. Bayat, P. Guerrero, M. Igartua, K. de la Caba, R.M. Hernandez, Development of bioinspired gelatin and gelatin/chitosan bilayer hydrofilms for wound healing, Pharmaceutics (2019).
[26] H. Samadian, A. Ehterami, A. Sarrafzadeh, H. Khastar, M. Nikbakht, A. Rezaei, L. Chegini, M. Salehi, Sophisticated polycaprolactone/gelatin nanofibrous nerve guided conduit containing platelet-rich plasma and citicoline for peripheral nerve regeneration: In vitro and in vivo study, Int. J. Biol. Macromol. 150 (2020) 380–388.
[27] N. Raina, R. Pahwa, J.K. Khosla, P.N. Gupta, M. Gupta, Polycaprolactone-based materials in wound healing applications, Polym. Bull. 79 (9) (2022) 7041–7063.
[28] F. Zhou, C. Cui, S. Sun, S. Wu, S. Chen, J. Ma, C.M. Li, Electrospun ZnO-loaded chitosan/PCL bilayer membranes with spatially designed structure for accelerated wound healing, Carbohydr. Polym. 282 (2022) 119131.
[29] S. Fahimirad, H. Abtahi, P. Satei, E. Ghaznavi-Rad, M. Moslehi, A. Ganji, Wound healing performance of PCL/chitosan based electrospun nanofiber electrosprayed with curcumin loaded chitosan nanoparticles, Carbohydr. Polym. 259 (2021) 117640.
[30] E. Rezvani Ghomi, V. Chellappan, R.E. Neisiany, N. Dubey, K. Amuthavalli, N. K. Verma, R. Lakshminarayanan, S. Ramakrishna, An innovative tunable bimodal porous PCL/gelatin dressing fabricated by electrospinning and 3D printing for efficient wound healing and scalable production, Compos. Sci. Technol. 247 (2024) 110402.
[31] X. Du, L. Li, J. Li, C. Yang, N. Frenkel, A. Welle, S. Heissler, A. Nefedov, M. Grunze, P.A. Levkin, UV-triggered dopamine polymerization: control of polymerCCon, Surface Coating, and Photopatterning, Adv. Mater. 26 (47) (2014) 8029–8033.
[32] V. Mayandi, A.C. Wen Choong, C. Dhand, F.P. Lim, T.T. Aung, H. Sriram, N. Dwivedi, M.H. Periayah, S. Sridhar, M.H.U.T. Fazil, E.T.L. Goh, G. Orive, R. W. Beuerman, T.M.S. Barkham, X.J. Loh, Z.-X. Liang, V.A. Barathi, S. Ramakrishna, S.J. Chong, N.K. Verma, R. Lakshminarayanan, Multifunctional antimicrobial nanofiber dressings containing ε-polylysine for the eradication of bacterial bioburden and promotion of wound healing in critically colonized wounds, ACS Appl. Mater. Interfaces 12 (14) (2020) 15989–16005.
[33] H. Chen, Y.S. Lui, Z.W. Tan, J.Y.H. Lee, N.S. Tan, L.P. Tan, Migration and phenotype control of human dermal fibroblasts by electrospun fibrous substrates, Adv. Healthc. Mater. 8 (9) (2019) 1801378.
[34] C.-C. Liang, A.Y. Park, J.-L. Guan, In vitro scratch assay: a convenient and inexpensive method for analysis of cell migration in vitro, Nat. Protoc. 2 (2) (2007) 329–333.
[35] T. Hodgkinson, X.-F. Yuan, A. Bayat, Electrospun silk fibroin fiber diameter influences in vitro dermal fibroblast behavior and promotes healing of ex vivo wound models, J. Tissue Engin. 5 (2014) 2041731414551661.
[36] S. Cui, B. Yao, M. Gao, X. Sun, D. Gou, J. Hu, Y. Zhou, Y. Liu, Effects of pectin structure and crosslinking method on the properties of crosslinked pectin nanofibers, Carbohydr. Polym. 157 (2017) 766–774.
[37] Y. Liu, S. Zhou, Y. Gao, Y. Zhai, Electrospun nanofibers as a wound dressing for treating diabetic foot ulcer, Asian J. Pharm. Sci. 14 (2) (2019) 130–143.
[38] Z. Kopecki, A.J. Cowin, The role of actin remodelling proteins in wound healing and tissue regeneration, wound healing-new insights into ancient challenge, IntechOpen (2016) 133–154.
[39] J. Wang, M. Windbergs, Functional electrospun fibers for the treatment of human skin wounds, Eur. J. Pharm. Biopharm. 119 (2017) 283–299.
[40] R.S. Vieira, M.L.M. Oliveira, E. Guibal, E. Rodríguez-Castellón, M.M. Beppu, Copper, mercury and chromium adsorption on natural and crosslinked chitosan films: an XPS investigation of mechanism, Colloids Surf A Physicochem Eng Asp 374 (1) (2011) 108–114.
[41] K. Jalaja, P.R.A. Kumar, T. Dey, S.C. Kundu, N.R. James, Modified dextran cross-linked electrospun gelatin nanofibres for biomedical applications, Carbohydr. Polym. 114 (2014) 467–475.
[42] J. Hua, Z. Li, W. Xia, N. Yang, J. Gong, J. Zhang, C. Qiao, Preparation and properties of EDC/NHS mediated crosslinking poly (gamma-glutamic acid)/epsilon-polylysine hydrogels, Mater. Sci. Eng. C 61 (2016) 879–892.

[43] T.A. Khan, K.K. Peh, H.S. Ch'ng, Mechanical, bioadhesive strength and biological evaluations of chitosan films for wound dressing, J. Pharm. Pharm. Sci. 3 (3) (2000) 303–311.
[44] Z. Yu, G. Rao, Y. Wei, J. Yu, S. Wu, Y. Fang, Preparation, characterization, and antibacterial properties of biofilms comprising chitosan and ε-polylysine, Int. J. Biol. Macromol. 141 (2019) 545–552.
[45] Y.Z. Zhang, J. Venugopal, Z.M. Huang, C.T. Lim, S. Ramakrishna, Crosslinking of the electrospun gelatin nanofibers, Polymer 47 (8) (2006) 2911–2917.
[46] L. Ghasemi-Mobarakeh, M.P. Prabhakaran, M. Morshed, M.-H. Nasr-Esfahani, S. Ramakrishna, Electrospun poly(ε-caprolactone)/gelatin nanofibrous scaffolds for nerve tissue engineering, Biomaterials 29 (34) (2008) 4532–4539.
[47] K. Ren, Y. Wang, T. Sun, W. Yue, H. Zhang, Electrospun PCL/gelatin composite nanofiber structures for effective guided bone regeneration membranes, Mater. Sci. Eng. C 78 (2017) 324–332.
[48] V. Albright, M. Xu, A. Palanisamy, J. Cheng, M. Stack, B. Zhang, A. Jayaraman, S. A. Sukhishvili, H. Wang, Micelle-coated, hierarchically structured nanofibers with dual-release capability for accelerated wound healing and infection control, Adv. Healthc. Mater. 7 (11) (2018) 1800132.
[49] P. Kanmani, J.-W. Rhim, Physical, mechanical and antimicrobial properties of gelatin based active nanocomposite films containing AgNPs and nanoclay, Food Hydrocoll. 35 (2014) 644–652.
[50] P. Rousselle, F. Braye, G. Dayan, Re-epithelialization of adult skin wounds: Cellular mechanisms and therapeutic strategies, Adv. Drug Deliv. Rev. 146 (2019) 344–365.
[51] A. Rai, R. Ferrão, P. Palma, T. Patricio, P. Parreira, E. Anes, C. Tonda-Turo, M.C. L. Martins, N. Alves, L. Ferreira, Antimicrobial peptide-based materials: opportunities and challenges, J. Mater. Chem. B 10 (14) (2022) 2384–2429.
[52] C.-Y. Huang, K.-H. Hu, Z.-H. Wei, Comparison of cell behavior on pva/pva-gelatin electrospun nanofibers with random and aligned configuration, Sci. Rep. 6 (1) (2016) 37960.
[53] S. Patel, K. Kurpinski, R. Quigley, H. Gao, B.S. Hsiao, M.-M. Poo, S. Li, Bioactive nanofibers: synergistic effects of nanotopography and chemical signaling on cell guidance, Nano Lett. 7 (7) (2007) 2122–2128.
[54] L. Sun, W. Gao, X. Fu, M. Shi, W. Xie, W. Zhang, F. Zhao, X. Chen, Enhanced wound healing in diabetic rats by nanofibrous scaffolds mimicking the basketweave pattern of collagen fibrils in native skin, Biomater. Sci. 6 (2) (2018) 340–349.
[55] G. Ajmal, G.V. Bonde, P. Mittal, G. Khan, V.K. Pandey, B.V. Bakade, B. Mishra, Biomimetic PCL-gelatin based nanofibers loaded with ciprofloxacin hydrochloride and quercetin: a potential antibacterial and anti-oxidant dressing material for accelerated healing of a full thickness wound, Int. J. Pharm. 567 (2019) 118480.